POZNAN UNIVERSITY OF TECHNOLOGY ACADEMIC JOURNALS
No 89 Electrical Engineering 2017

DOI 10.21008/j.1897-0737.2017.89.0008

Tomasz SZCZEGIELNIAK*
Dariusz KUSIAK*
Zygmunt PIĄTEK*

POWER LOSSES IN THE THREE-PHASE GAS-INSULATED LINE

This paper presents an analytical method for determining the power losses in the three–phase gas–insulated line (i.e., high-current busduct) of circular cross–section geometry which phase conductors are placed in vertex of a square. The mathematical model takes into account the skin effect and the proximity effects, as well as the complete electromagnetic coupling between phase conductors and enclosures (i.e., screens). The power losses produced by high-current busducts are usually calculated numerically with the use of a computer. However, the analytical calculation of the power losses is preferable, because it results in a mathematical expression for showing its dependences on various parameters of the line arrangement. Moreover, knowledge of the relations between electrodynamics and constructional parameters is necessary in the optimization construction process of the high-current busducts.

KEYWORDS: high-current busduct, electromagnetic field, power losses

1. INTRODUCTION

Following the development of thermal and hydroelectric power stations, at the beginning of the 30s, high-current transmission lines with screened busducts connecting big generators with unit transformers began to be installed. Due to the necessity of transmitting power becoming higher and higher, and to the environmental protection requirements, the length of the line was to be a few kilometers [1–9]. It is estimated that until now the length of the existing lines of that type has not surpassed 100 km. GILs used for high power transmission have been described several times, e.g. in Refs. [4, 5, 6, 8, 9, 10]. The gas most often used for insulation is SF_6 (sulphur hexafluoride) whose pressure values range from 0.29 to 0.51 MPa (at 20°C). Recently, SF_6 has been replaced with the 95% mixture of nitrogen N_2 and 5% of SF_6 of 1.3 MPa pressure, or with a 90% mixture of nitrogen N_2 and 10% of SF_6 of 0.94 MPa pressure, as well as with a 80%

* Częstochowa University of Technology.

mixture of nitrogen N_2 and 20% of SF_6 of 0.71 MPa pressure corresponding to the 0.4 MPa pressure in the case when pure SF_6 is used [1, 2, 3, 4, 5, 8, 9]. The contemporary solutions consist of transmission lines insulated with air at atmospheric pressure, with duty-rated voltage values reaching up to 36 kV and duty–rated current values reaching up to: 10 kA for hydroelectric power plants, 20 kA for thermal and nuclear plants whose duty–rated power values reach up to 900 MW, 31.5 kA for nuclear plants with power value of 1300 MW [1, 2, 4, 5, 8, 9]. Today high–current busducts are applied in many projects around the world when high–power transmission of high reliability and maximum availability is required. The sizes of new projects are constantly increasing: from some hundred meters to several kilometers [1, 2, 4, 5, 9]. The construction and assembling methods of GIL elaborated recently make it possible to build transmission lines over the ground and in underground tunnels or directly in the ground. Underground GIL, being large power transmission lines, are most commonly built in areas with dense house-dwelling where requirements concerning safety and environmental protection are very strict.

The design of the busducts used for high currents and voltages requires the precise analysis of electromagnetic, dynamic and thermal effects. Knowledge of the relations between electrodynamics and constructional parameters is necessary in the optimization construction process of the high-current busducts [1–9].

Power losses depend on value of currents, and for the large cross-sectional dimensions of the phase conductor, even at industrial frequency, skin, external (Fig. 1) and internal (Fig. 2) proximity effect should be taken into account [2, 9].

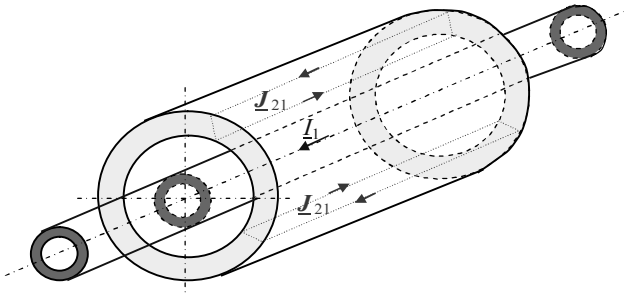

Fig. 1. Eddy currents induced in the screen by the magnetic field of the own current of the phase conductor

The most popular solution of the high current busducts are symmetrical or flat [2, 9]. In this paper the analytical calculations of the power losses in the high current busduct which phase conductors are placed in vertex of a square will be presented (Fig. 3).

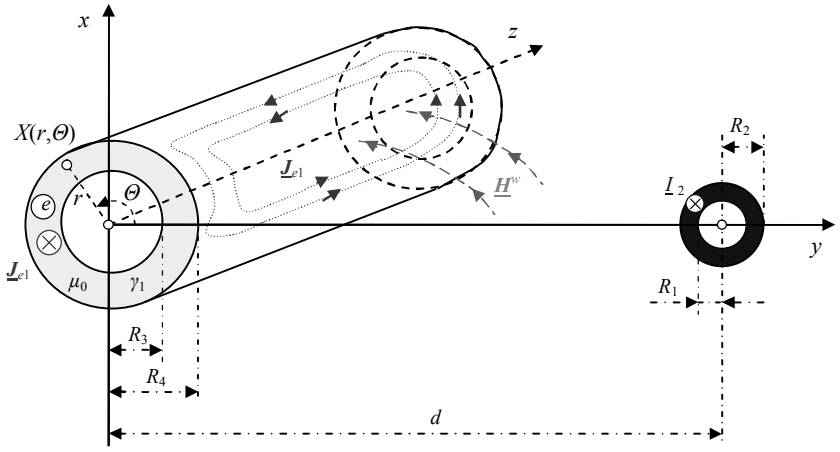

Fig. 2. Eddy currents induced in the screen by the magnetic field of the neighboring phase conductor

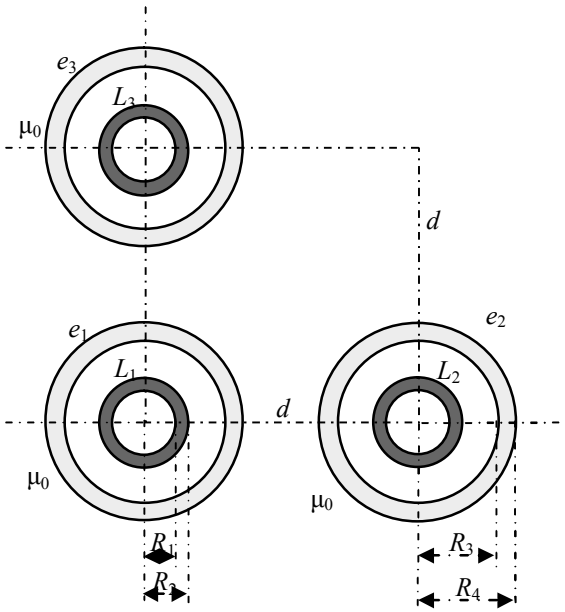

Fig. 3. Three-phase high-current busduct which phase conductors are placed in vertex of a square

Presented in the figure 3 system of tubular conductors is the most often installed when symmetrical or flat high-current busduct can not be used. This situation appears in the narrow tunnels, shafts, cable ducts (Fig. 4).

Fig. 4. High current busduct in the power plant. Reproduced by permission of Holduct Ltd [10]

2. ELECTROMAGNETIC FIELD

Let us consider the electromagnetic field in a three-pole high-current busduct presented in the Fig. 3. Using the Laplace's and Helmoltz's equations we can determine the electromagnetic field in the conductors and the screens [2, 9]. The total current density in the first screen e_1 is a sum of currents induced by each conductor, that is to say

$$\underline{J}_{e1}(r,\Theta) = \underline{J}_{e11}(r,\Theta) + \underline{J}_{e12}(r,\Theta) + \underline{J}_{e13}(r,\Theta) = \underline{J}_{e11}(r,\Theta) + \underline{J}_{e123}(r,\Theta) \quad (1)$$

For the positive sequence of currents, i.e.

$$\underline{I}_2 = \exp[-\mathrm{j}\frac{2}{3}\pi]\,\underline{I}_1 \quad \text{and} \quad \underline{I}_3 = \exp[\mathrm{j}\frac{2}{3}\pi]\,\underline{I}_1 \quad (2)$$

the current density $\underline{J}_{e1}(r,\Theta)$ is defined by Eq. (1) in which

$$\underline{J}_{e11}(r) = \frac{\underline{\Gamma}_e\,\underline{I}_1}{2\pi R_3}\,\underline{j}_{e0}(r) = \frac{\underline{\Gamma}_e\,\underline{I}_1}{2\pi R_3}\,\frac{\underline{b}_0\,I_0(\underline{\Gamma}_e\,r) + \underline{c}_0\,K_0(\underline{\Gamma}_e\,r)}{\underline{d}_0} \quad (3)$$

where

$$\underline{d}_0 = I_1(\underline{\Gamma}_e R_4)\,K_1(\underline{\Gamma}_e R_3) - I_1(\underline{\Gamma}_e R_3)\,K_1(\underline{\Gamma}_e R_4) \quad (3a)$$

$$\underline{b}_0 = \beta_e\,K_1(\underline{\Gamma}_e R_3) - K_1(\underline{\Gamma}_e R_4) \quad (3b)$$

$$\underline{c}_0 = \beta_e\,I_1(\underline{\Gamma}_e R_3) - I_1(\underline{\Gamma}_e R_4) \quad (3c)$$

whereas current density $\underline{J}_{e123}(r,\Theta)$ can be expressed as follows

$$\underline{J}_{e123}(r,\Theta) = \underline{J}_{e12}(r,\Theta) + \underline{J}_{e13}(r,\Theta) = -\frac{\underline{\Gamma}_e\,\underline{I}_1}{\pi\,R_4}\sum_{n=1}^{\infty}\underline{D}_n\left(\frac{R_4}{d}\right)^n\underline{f}_{ne}(r) \quad (4)$$

where

$$\underline{D}_n = \exp\left[-\mathrm{j}\frac{2}{3}\pi\right]\cos n\Theta + \exp\left[\mathrm{j}\frac{2}{3}\pi\right]\cos n\left(\Theta - \frac{\pi}{2}\right) \tag{4a}$$

and

$$\underline{f}_{ne}(r) = \frac{K_{n+1}(\underline{\Gamma}_e R_3)\, I_n(\underline{\Gamma}_e r) + I_{n+1}(\underline{\Gamma}_e R_3)\, K_n(\underline{\Gamma}_e r)}{I_{n-1}(\underline{\Gamma}_e R_4)\, K_{n+1}(\underline{\Gamma}_e R_3) - I_{n+1}(\underline{\Gamma}_e R_3)\, K_{n-1}(\underline{\Gamma}_e R_4)} \tag{4b}$$

The current density in the second screen e_2 are defined by Eq. (1) respectively, in which current $\underline{I}_1$ should be replaced with $\underline{I}_2$ and constant $\underline{D}_n$ with constant

$$\underline{G}_n = (-1)^n \left\{\exp\left[\mathrm{j}\frac{2}{3}\pi\right]\cos n\Theta + \left(\frac{1}{\sqrt{2}}\right)^n \exp\left[-\mathrm{j}\frac{2}{3}\pi\right]\cos n\left(\Theta + \frac{\pi}{4}\right)\right\} \tag{5}$$

Formulas for screen e_3 are obtained in the same way by replacing $\underline{I}_1$ and $\underline{D}_n$, respectively, with $\underline{I}_3$ and

$$\underline{M}_n = (-1)^n \exp\left[-\mathrm{j}\frac{2}{3}\pi\right]\cos n\left(\Theta - \frac{\pi}{2}\right) + \left(\frac{1}{\sqrt{2}}\right)^n \exp\left[\mathrm{j}\frac{2}{3}\pi\right]\cos n\left(\Theta + \frac{\pi}{4}\right) \tag{6}$$

In the above formulas, $I_0(\underline{\Gamma}_e r)$, $K_0(\underline{\Gamma}_e r)$, $I_1(\underline{\Gamma}_e r)$, $K_1(\underline{\Gamma}_e r)$, $I_n(\underline{\Gamma}_e r)$, $K_n(\underline{\Gamma}_e r)$, $I_{n-1}(\underline{\Gamma}_e r)$, $K_{n-1}(\underline{\Gamma}_e r)$, $I_{n+1}(\underline{\Gamma}_e r)$ and $K_{n+1}(\underline{\Gamma}_e r)$ are the modified Bessel's functions of order 0, 1, n, n–1 and n+1, calculated for $r = R_3$ and $r = R_4$ [11], and the complex propagation constant of electromagnetic wave in the screen equals

$$\underline{\Gamma}_e = \sqrt{\mathrm{j}\omega\mu_0\gamma_e} = \sqrt{\omega\mu_0\gamma_e}\,\exp[\mathrm{j}\frac{\pi}{4}] = k_e + \mathrm{j}\,k_e = \sqrt{2\mathrm{j}}\,k_e \tag{7}$$

with the attenuation constant

$$k_e = \sqrt{\frac{\omega\mu_0\gamma_e}{2}} = \frac{1}{\delta} \tag{8}$$

where δ is the electrical skin depth of the electromagnetic wave penetration into the conducting environment, ω is the angular frequency, γ_e stands for the conductivity of the screen, and $\mu_0 = 4\pi\,10^{-7}\ \mathrm{H\cdot m^{-1}}$ is the magnetic permeability of the vacuum.

Inside the phase conductors ($R_1 \le r \le R_2$) of the high current busduct the current density equals [2, 9]

$$\underline{J}_{11}(r) = \frac{\underline{\Gamma}\,\underline{I}_1}{2\pi R_2}\,\frac{K_1(\underline{\Gamma}R_1)\,I_0(\underline{\Gamma}r) + I_1(\underline{\Gamma}R_1)\,K_0(\underline{\Gamma}r)}{I_1(\underline{\Gamma}R_2)\,K_1(\underline{\Gamma}R_1) - I_1(\underline{\Gamma}R_1)\,K_1(\underline{\Gamma}R_2)} \tag{9}$$

The complex propagation constant in the conductors is $\underline{\Gamma} = \sqrt{\mathrm{j}\omega\mu_0\gamma}$, and γ is the conductivity of the phase conductor.

3. POWER LOSSES

Power losses in the three-phase gas-insulated lines can be determined with Poynting theorem. But if we use Poynting theorem, we can not isolate the real part (as an active power) and the imaginary part (as a reactive power). It is hard on account of the complex propagation constant and complex modified Bessel's functions. Therefore, the active power (power losses) will be calculated from Joule-Lenz law [1, 2, 9]:

$$P = \iiint_V \frac{1}{\gamma} \underline{J}(r)\, \underline{J}^*(r)\, \mathrm{d}V \tag{10}$$

Power losses in the conductors of the single–pole high–current transmission line presented in the figure 3 are expressed by formula:

$$P_C = \frac{\underline{\Gamma}\, l\, I_1^2}{4\,\pi\,\gamma\, R_2} \frac{\underline{a}}{\underline{b}\,\underline{b}^*} \tag{11}$$

in which

$$\begin{aligned} \underline{a} = {} & K_1(\underline{\Gamma}R_1)\, K_1^*(\underline{\Gamma}R_1) \begin{bmatrix} I_0(\underline{\Gamma}R_2)\, I_1^*(\underline{\Gamma}R_2) - \\ j\, I_1(\underline{\Gamma}R_2)\, I_0^*(\underline{\Gamma}R_2) \end{bmatrix} \\ & - I_1(\underline{\Gamma}R_1)\, I_1^*(\underline{\Gamma}R_1) \begin{bmatrix} K_0(\underline{\Gamma}R_2)\, K_1^*(\underline{\Gamma}R_2) - \\ j\, K_1(\underline{\Gamma}R_2)\, K_0^*(\underline{\Gamma}R_2) \end{bmatrix} \\ & + I_1(\underline{\Gamma}R_1)\, K_1^*(\underline{\Gamma}R_1) \begin{bmatrix} K_0(\underline{\Gamma}R_2)\, I_1^*(\underline{\Gamma}R_2) + \\ j\, K_1(\underline{\Gamma}R_2)\, I_0^*(\underline{\Gamma}R_2) \end{bmatrix} \\ & - K_1(\underline{\Gamma}R_1)\, I_1^*(\underline{\Gamma}R_1) \begin{bmatrix} I_0(\underline{\Gamma}R_2)\, K_1^*(\underline{\Gamma}R_2) + \\ j\, I_1(\underline{\Gamma}R_2)\, K_0^*(\underline{\Gamma}R_2) \end{bmatrix} \end{aligned} \tag{11a}$$

$$\underline{b} = I_1(\underline{\Gamma}\,R_2)\, K_1(\underline{\Gamma}\,R_1) - I_1(\underline{\Gamma}\,R_1)\, K_1(\underline{\Gamma}\,R_2) \tag{11b}$$

$$\underline{b}^* = I_1^*(\underline{\Gamma}\,R_2)\, K_1^*(\underline{\Gamma}\,R_1) - I_1^*(\underline{\Gamma}\,R_1)\, K_1^*(\underline{\Gamma}\,R_2) \tag{11c}$$

In turn, power losses in the outer screens (e_2 and e_3) are the same and can be write down as follows:

$$P_{e2} = P_{e3} = P_{e0} + P_{e23} \tag{12}$$

where

$$P_{e0} = \frac{\underline{\Gamma}_e^*\, l\, {I_1}^2}{4\,\pi\,\gamma_e\,\beta_e^2\, R_4} \frac{\underline{a}_0}{\underline{d}_0\,\underline{d}_0^*} \tag{13}$$

in which

$$\begin{aligned}\underline{a}_0 = \underline{b}_0\,\underline{b}_0^*&\left\{\begin{matrix} I_0^*(\underline{\Gamma}_e R_4) I_1(\underline{\Gamma}_e R_4) + j\, I_0(\underline{\Gamma}_e R_4) I_1^*(\underline{\Gamma}_e R_4) - \\ \beta_e\left[I_0^*(\underline{\Gamma}_e R_3) I_1(\underline{\Gamma}_e R_3) + j\, I_0(\underline{\Gamma}_e R_3) I_1^*(\underline{\Gamma}_e R_3)\right]\end{matrix}\right\} \\ -\underline{c}_0\,\underline{c}_0^*&\left\{\begin{matrix} K_0^*(\underline{\Gamma}_e R_4) K_1(\underline{\Gamma}_e R_4) + j\, K_0(\underline{\Gamma}_e R_4) K_1^*(\underline{\Gamma}_e R_4) - \\ \beta_e\left[K_0^*(\underline{\Gamma}_e R_3) K_1(\underline{\Gamma}_e R_3) + j\, K_0(\underline{\Gamma}_e R_3) K_1^*(\underline{\Gamma}_e R_3)\right]\end{matrix}\right\} \\ -\underline{c}_0\,\underline{b}_0^*&\left\{\begin{matrix} I_0^*(\underline{\Gamma}_e R_4) K_1(\underline{\Gamma}_e R_4) - j\, K_0(\underline{\Gamma}_e R_4) I_1^*(\underline{\Gamma}_e R_4) - \\ \beta_e\left[I_0^*(\underline{\Gamma}_e R_3) K_1(\underline{\Gamma}_e R_3) - j\, K_0(\underline{\Gamma}_e R_3) I_1^*(\underline{\Gamma}_e R_3)\right]\end{matrix}\right\} \\ +\underline{b}_0\,\underline{c}_0^*&\left\{\begin{matrix} I_1(\underline{\Gamma}_e R_4) K_0^*(\underline{\Gamma}_e R_4) - j\, I_0(\underline{\Gamma}_e R_4) K_1^*(\underline{\Gamma}_e R_4) - \\ \beta_e\left[I_1(\underline{\Gamma}_e R_3) K_0^*(\underline{\Gamma}_e R_3) - j\, I_0(\underline{\Gamma}_e R_3) K_1^*(\underline{\Gamma}_e R_3)\right]\end{matrix}\right\}\end{aligned} \tag{13a}$$

$$\underline{b}_0^* = \beta_e\, K_1^*(\underline{\Gamma}_e R_3) - K_1^*(\underline{\Gamma}_e R_4) \tag{13b}$$

$$\underline{c}_0^* = \beta_e\, I_1^*(\underline{\Gamma}_e R_3) - I_1^*(\underline{\Gamma}_e R_4) \tag{13c}$$

$$\underline{d}_0^* = I_1^*(\underline{\Gamma}_e R_4) K_1^*(\underline{\Gamma}_e R_3) - I_1^*(\underline{\Gamma}_e R_3) K_1^*(\underline{\Gamma}_e R_4) \tag{13d}$$

and

$$P_{e23} = \frac{\underline{\Gamma}_e^*\, l\, I_1^2}{2\pi\,\gamma\, R_4} \sum_{n=1}^{\infty}\left(1 + \left[\frac{1}{\sqrt{2}}\right]^{2n}\right)\left(\frac{R_4}{d}\right)^{2n} \frac{\underline{a}_{ne}}{\underline{b}_{ne}\,\underline{b}_{ne}^*} \tag{14}$$

where

$$\begin{aligned}\underline{a}_{ne} = {} & I_{n+1}(\underline{\Gamma}_e R_4)\, K_{n+1}(\underline{\Gamma}_e R_3)\left[I_{n+1}^*(\underline{\Gamma}_e R_3)\, K_n^*(\underline{\Gamma}_e R_4) + I_n^*(\underline{\Gamma}_e R_4)\, K_{n+1}^*(\underline{\Gamma}_e R_3)\right] + \\ & + \mathrm{j}\, I_n(\underline{\Gamma}_e R_4)\, K_{n+1}(\underline{\Gamma}_e R_3)\left[I_{n+1}^*(\underline{\Gamma}_e R_4)\, K_{n+1}^*(\underline{\Gamma}_e R_3) - I_{n+1}^*(\underline{\Gamma}_e R_3)\, K_{n+1}^*(\underline{\Gamma}_e R_4)\right] - \\ & - I_{n+1}(\underline{\Gamma}_e R_3)\left\{\begin{matrix} K_{n+1}^*(\underline{\Gamma}_e R_3)\left[I_n^*(\underline{\Gamma}_e R_4)\, K_{n+1}(\underline{\Gamma}_e R_4) - \mathrm{j}\, I_{n+1}^*(\underline{\Gamma}_e R_4)\, K_n(\underline{\Gamma}_e R_4)\right] + \\ + I_{n+1}^*(\underline{\Gamma}_e R_3)\left[K_n^*(\underline{\Gamma}_e R_4)\, K_{n+1}(\underline{\Gamma}_e R_4) + \mathrm{j}\, K_{n+1}^*(\underline{\Gamma}_e R_4)\, K_n(\underline{\Gamma} R_4)\right]\end{matrix}\right\}\end{aligned} \tag{14a}$$

$$\underline{b}_{ne} = I_{n-1}(\underline{\Gamma}_e R_4)\, K_{n+1}(\underline{\Gamma}_e R_3) - I_{n+1}(\underline{\Gamma}_e R_3)\, K_{n-1}(\underline{\Gamma}_e R_4) \tag{14b}$$

$$\underline{b}_{ne}^* = I_{n-1}^*(\underline{\Gamma}_e R_4)\, K_{n+1}^*(\underline{\Gamma}_e R_3) - I_{n+1}^*(\underline{\Gamma}_e R_3)\, K_{n-1}^*(\underline{\Gamma}_e R_4) \tag{14c}$$

Power losses in the first screen (e_1) are

$$P_{e1} = P_{e0} + P_{e123} \tag{15}$$

where

$$P_{e123} = \frac{\underline{\Gamma}_e^*\, l\, I_1^2}{\pi\,\gamma\, R_4} \sum_{n=1}^{\infty}\left(\frac{R_4}{d}\right)^{2n} \frac{\underline{a}_{ne}}{\underline{b}_{ne}\,\underline{b}_{ne}^*} \tag{16}$$

4. NUMERICAL EXAMPLE

Based on the derived formulae, the power losses in the high–current transmission lines depicted in figure 3 were calculated. According to the notation applied in figure 3, the following geometry of the busduct has been selected: $R_1 = 100$ mm, $R_2 = 110$ mm, $R_3 = 235$ mm, $R_4 = 240$ mm, $d = 640$ mm. Both the phase conductors and the screen are made of aluminium, which has an electric conductivity of $\gamma = 33$ MS·m^{-1}. The frequency is 50 Hz. Currents in the phase conductors are $\underline{I}_1 = 4000$ A, $\underline{I}_2 = 4000\exp[-j\frac{2}{3}\pi]$ A, $\underline{I}_3 = 4000\exp[j\frac{2}{3}\pi]$ A. The length of the busduct system is assumed to be $l = 10000$ mm. The results of the calculations are shown in Table 1.

Apart from analytical calculation, computer simulations for high–current busduct system power losses were also performed with the aid of the commercial FEMM software [12], using two-dimensional finite elements. Figure 5 shows the computational finite element mesh for single-pole high-current transmission line.

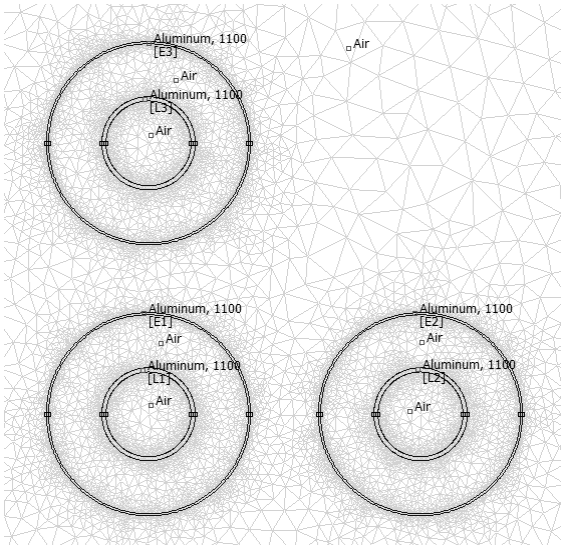

Fig. 5. The finite element mesh used in FEMM computations

5. CONCLUSIONS

An analytical approach to the solution of the power losses in the three-phase high-current busduct has been presented in this paper. The proposed method allows us to calculate the power losses in a set tubular busbars. The

mathematical model takes into account the skin effect and the proximity effects, as well as the complete electromagnetic coupling between phase conductors and screens. To verify the analytical formulae we performed computations by means of the finite element method.

As table 1 shows, the power losses calculated on the basis analytical formulae and power losses determined by FEMM software are almost the same especially for phase conductors. In general, the relative error does not exceed 20% for considered busduct. It is noticeable that the analytical calculated values are slightly smaller than the computed ones. The increased values probably come from that in the analytical model, phase conductors are considered as a system of parallel filaments.

Table 1. Power losses of the three-phase gas-insulated line

Region	Analytical calculation	FEMM computations
Phase L_1	731.07 W	733.37 W
Phase L_2	731.07 W	731.93 W
Phase L_3	731.07 W	732.05 W
Screen e_1	401.89 W	478.13 W
Screen e_2	295.87 W	197.17 W
Screen e_3	295.87 W	223.71 W

An analytical method presented in the paper can be used only for circular high current busducts. But numerical method can be used almost for all types of busducts.

In the paper using the Joule-Lenz law the active power (power losses) in the three-phase high-current busduct were determined. Using the Poynting theorem we can determine apparent power. On the basis of determined active and apparent power from Poynting theorem we can determine the reactive power emitted in the phase conductors and screens of the three-phase high-current busducts. But we should add that reactive power determined from Poynting theorem is connected with internal inductances of the screens and phase conductors.

REFERENCES

[1] Nawrowski R.: Tory wielkoprądowe izolowane powietrzem lub SF_6. Wyd. Pol. Poznańskiej, Poznań 1998.

[2] Piątek Z.: Impedances of high–current busducts. Wyd. Pol. Częst., Czestochowa 2008.

[3] Bednarek K., Nawrowski R., Tomczewski A.: Trójfazowe tory wielkoprądowe złożone z przewodów rurowych w indywidualnych osłonach. XVII Symp. PTZE, Rydzyna 2007, str. 21–23.
[4] CIGRE TB 218.: Gas Insulated Transmission Lines (GIL, CIGRE, Paris, France, 2003.
[5] CIGRE TB 351.: Application of Long High Capacity Gas Insulated Lines (GIL), CIGRE, Paris, France, 2008.
[6] Koch, H.: Gas–Insulated Transmission Lines (GIL). John Wiley & Sons, 2012.
[7] Piątek, Z.; Self and mutual impedances of a finite length gas insulated transmission line (GIL). Electric Power Systems Research, 2007**,** 77, 191–203.
[8] Sarajcev, P.; Numerical Analysis of the magnetic field of High–Current Busduct and GIL Systems. Energies 2011, 4, 2196–2211.
[9] Szczegielniak, T. Power Losses of the Screened and Unscreened Tubular High–Current Busduct. Doctoral, Silesian University of Technology, Gliwice 2011.
[10] Holduct Ltd. Three–phase busduct; Poland Available online: http://energetyka.holduct.com.pl.
[11] Mc Lachlan N.W.: Bessel functions for engineers (in Polish). 2nd ed.; PWN, Warsaw 1964.
[12] Meeker, D.C., Finite Element Method Magnetics, version 4.2 (11apr2012, Mathematica Build), http://www.femm.info.

(Received: 26. 01. 2017, revised: 15. 02. 2017)